J Mater Sci (2015) 50:5328–5336
DOI 10.1007/s10853-015-9080-3

Lead-free electrostrictive $(Bi_{0.5}Na_{0.5})TiO_3$–$(Bi_{0.5}K_{0.5})TiO_3$–$(K_{0.5}Na_{0.5})NbO_3$ ceramics with good thermostability and fatigue-free behavior

Jigong Hao[1] · Zhijun Xu[1] · Ruiqing Chu[1] · Wei Li[1] · Juan Du[1]

Received: 3 January 2015 / Accepted: 5 May 2015 / Published online: 12 May 2015

Abstract In this study, we designed a series of compositions deep in pseudocubic region based on ternary $(1-x)[(1-y)(Bi_{0.5}Na_{0.5})TiO_3$–$y(Bi_{0.5}K_{0.5})TiO_3]$–$x(K_{0.5}Na_{0.5})NbO_3$ (BNKT100y–100xKNN) system for electrostrictive applications. Results show that the KNN substitution into BNKT100y induces a significant disruption of the ferroelectric order, and tends to enhance the electrostrictive properties of the ceramics. A high, purely electrostrictive effect with large electrostrictive coefficient Q_{33} of 0.025 m^4/C^2 and good thermostability comparable with that of traditional Pb-based electrostrictors is obtained for BNKT100y–xKNN ($y = 0.20$, $x = 0.16$) ceramics, which lies deep in pseudocubic region along the MPB compositions of the ternary system. Temperature-dependent structural analysis suggests that the good electrostrictive properties insensitive to temperature can be ascribed to the stable relaxor pseudocubic phase over a wide temperature range. Furthermore, it is found that the electrostrictive coefficient Q_{33} exhibits only small degradation within 2 % at the field amplitude of 80 kV/cm up to 10^5 switching cycles. The large and purely electrostrictive effect with the exceptionally good fatigue resistance and thermostability makes this material a great potential to be applied to the environmental-friendly solid-state actuators.

✉ Zhijun Xu
zhjxu@lcu.edu.cn

Jigong Hao
haojigong@163.com

[1] College of Materials Science and Engineering, Liaocheng University, Liaocheng 252059, People's Republic of China

Introduction

Electrostriction is the dependence of the state of strain of dielectrics upon the even powers of the applied electric field. In electrostriction, the sign of the field-induced deformation is independent of the polarity of the field and is proportional to the square of the applied electric field $S = QP^2$, where Q is the electrostrictive coefficient and P is polarization [1]. Materials such as relaxor $Pb(Mg_{1/3}Nb_{2/3})O_3$ (PMN) demonstrate large electrostrictive strain, which is known as the best electrostrictive material and widely used in actuator applications [2, 3]. However, lead is toxic, hence making lead-free electrostrictive materials highly desirable owing to the focus of the global environmental problems and the increasing concern for environmental safety.

In typical ferroelectrics, electrostriction is significantly large just above the Curie temperature, where an electric field can induce energetically unstable ferroelectric phase [4]. By contrast, relaxor ferroelectrics can exhibit a relatively high electrostrictive strain in a wide temperature range due to the diffused phase transition [1]. If the phase transition temperature is close to room temperature (RT), the electrostrictive effect can be very large at RT [5]. Therefore, one may adjust the composition in lead-free relaxor ferroelectrics to achieve pseudocubic/cubic crystal structure at RT, which might produce good lead-free electrostrictors. Based on the above, Zhang et al. [5, 6] proposed a new concept of using lead-free BNT-based "antiferroelectrics" (AFE) as electrostrictors, which can provide high strain and minimal losses at RT combined with weak temperature dependence. Such a concept has also been proposed in lead-free KNN-based [7] and $SrTiO_3$-based materials [8].

Very recently, we disclosed that ternary $(Bi_{0.5}Na_{0.5})TiO_3$–$(Bi_{0.5}K_{0.5})TiO_3$–$(K_{0.5}Na_{0.5})NbO_3$ (BNT–BKT–KNN)

system near the morphotropic phase boundary (MPB) exhibited a high electrostrictive response comparable with that of traditional Pb-based electrostrictors [9], which suggests that these lead-free electrostrictors are very promising for practical applications by replacing Pb-based materials. However, one drawback for the use as material for piezoelectric devices is the huge intrinsic losses due to the large hysteresis near the MPB. Therefore, electric-field-induced strain is generally required to be accompanied with low hysteresis so as to improve the sensitivity. Moreover, practical applications demand not only outstanding electrostrictive properties but also the reliability and long-term stability during cyclic electric loading to ensure successful industrial implementation. Besides, thermal stability of BNT-based electrostrictors is also practically important for highly reliable precision mechatronic systems [10]. Our previous study found that the high-performance BNT–BKT–KNN ceramics near the MPB exhibit quite poor electrostrictive fatigue properties, with relatively severe degradation in strain behavior after only a few millions of cycles of applied field. Furthermore, the materials suffer from large hysteresis loss, which impedes the practical applications of the materials. Therefore, there is great need to improve the fatigue characteristics and reduce the hysteresis while maintaining good temperature stability.

In this study, based on the MPB composition of BNT–BKT–KNN ceramics, we designed a series of compositions which lie deep in the pseudocubic region of ternary BNT–BKT–KNN system, as indicated in the phase diagram of this system depicted in our recent work (Fig. 1) [11]. By changing the content of BKT and KNN, a high, purely electrostrictive effect was developed in the ternary BNT–BKT–KNN system, which can deliver an exceptionally good fatigue resistance and provide temperature independence of strain, indicating great potential in environmental-friendly solid-state actuators.

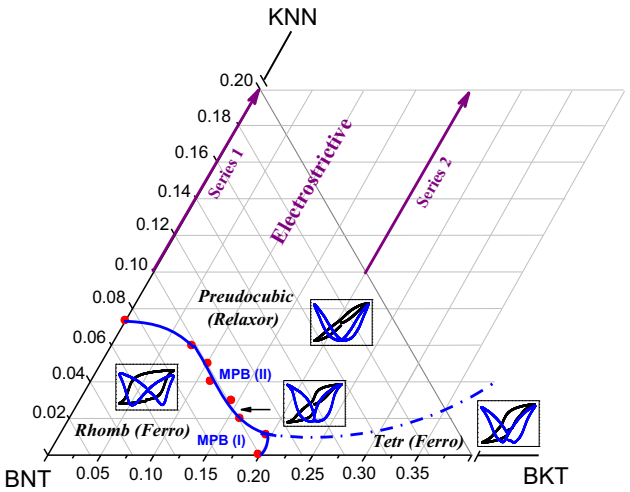

Fig. 1 Phase diagram of ternary BNT–BKT–KNN system reported in our recent work [11] and the designed compositions in this study based on the system

Experimental procedure

$(1-x)[(1-y)(Bi_{0.5}Na_{0.5})TiO_3–y(Bi_{0.5}K_{0.5})TiO_3]–x(K_{0.5}Na_{0.5})NbO_3$ (abbreviate as BNKT100*y*–100*x*KNN, series 1, $y = 0$, $x = 0.10$–0.20; series 2, $y = 0.20$, $x = 0.10$–0.20) were prepared by a conventional ceramic fabrication process using reagent-grade metal oxides or carbonate powders of Na_2CO_3 (99.95 %), K_2CO_3 (99.5 %), Nb_2O_5 (99 %), TiO_2 (99.6 %), and Bi_2O_3 (99.975 %) as raw materials. BNKT100*y* ($y = 0$, 0.20) and KNN powders were first calcined at 850 and 880 °C for 4 h, respectively. Subsequently, the above powders were weighted according to the formulas and then mixed and crashed by planetary ball-milling with a rotation speed of 330r/min in a polyethylene with ZrO_2 balls for 24 h using ethanol as the medium. The resulting powders were then mixed with 10 % polyvinyl alcohol (PVA), and pressed into pellets of 10 mm diameter and 0.7–1.0 mm thickness by uniaxial pressing at 100 MPa. These pellets were finally sintered in air at 1150–1170 °C for 2 h in air. The crystal structures of the sintered ceramics were determined by X-ray powder diffraction analysis (XRD) (D8 Advance, Bruker Inc., Germany). For the temperature-dependent structural analysis, a reflective XRD apparatus (Bruker D8 Advance) equipped with a furnace (XRK900) was used using Cu K_a radiation. The surface morphology of the ceramics was studied by scanning electron microscope (SEM) (JSM-5900, Japan).

For the electrical measurements, silver paste was coated on both sides of the sintered samples and fired at 650 °C for 10 min to form electrodes. The temperature dependences of the dielectric properties were measured using an Agilent 4294A precision impedance analyzer (Agilent Inc., USA). Impedance spectroscopy of the samples was performed using a broad frequency dielectric spectrometer (Concept80, Novocontrol Inc., Germany) in the 0.01 Hz–20 MHz frequency range at various temperatures. The electric-field-induced polarization (*P*–*E*), strain (*S*–*E*), large signal piezoelectric coefficient (d^*_{33}–*E*), and permittivity (ε_r–*E*) measurements were carried out using an aix-ACCT TF2000FE-HV ferroelectric test unit (aix-ACCT Inc., Germany) connected with a miniature plane mirror interferometer and the accessory laser interferometer vibrometer (SP-S 120/500; SIOS Mebtechnik GmbH, llmenau, Germany).

Results and discussion

Figure 2 presents the XRD patterns of the sintered and then crushed samples of BNKT100*y*–100*x*KNN ($y = 0$, 0.20; $x = 0.10$–0.20) ceramics, which show a single perovskite

structure without apparent trace of secondary phases. All the peaks could be indexed based on a pseudocubic perovskite structure as evident by the undetected splitting of any of the peaks [12], confirming the designed compositions are in the pseudocubic region of the ternary BNT–BKT–KNN system.

Figure 3a, b provides micrographs of the BNKT100*y*–100*x*KNN [(a) $y = 0$, $x = 0.10$; (b) $y = 0$; $x = 0.20$)] ceramic representing the typical microstructure observed throughout all the compositions. The microstructure appears homogeneous and almost fully dense without any apparent second phase. By applying the Archimedes method, all samples have a large relative density of >95 %. The average grain size decreases monotonically as the KNN content increases (Fig. 3c), which implies that the role of KNN in BNT-based system is a grain growth inhibiter [12].

Figure 4 shows frequency dispersion of the dielectric properties of BNKT100*y*–100*x*KNN ceramics. All indicated samples show evidence of diffuse phase transition, which is typical for relaxor ferroelectrics. Two obvious dielectric anomalies which correspond to T_s at low temperature and T_m at high temperature, respectively, are

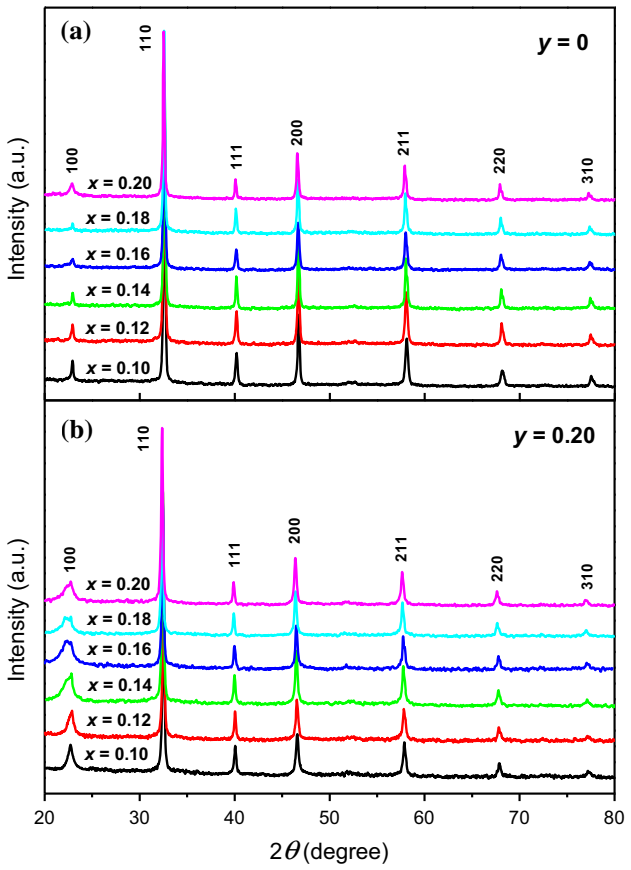

Fig. 2 XRD patterns of the BNKT100*y*–*x*KNN (**a** $x = 0.10$–0.20, $y = 0$; **b** $x = 0.10$–0.20, $y = 0.20$) ceramics

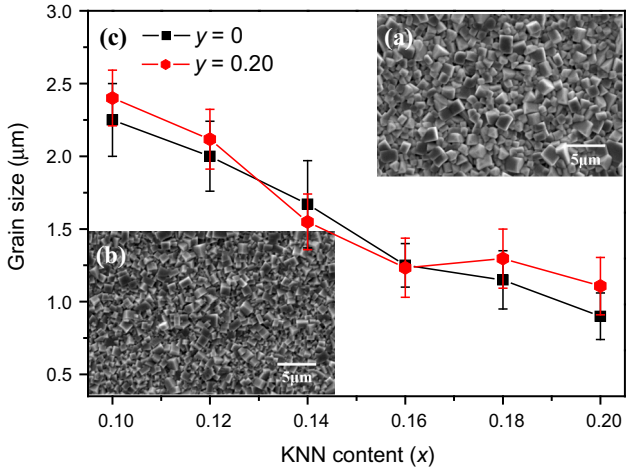

Fig. 3 The micrographs of the BNKT100*y*–*x*KNN (*a* $y = 0$, $x = 0.10$; *b* $y = 0$; $x = 0.20$). *c* Average grain size of BNKT100*y*–*x*KNN ceramics as a function of KNN content

exhibited by these materials. In addition, the temperature dependence of the dielectric permittivity in these materials reflects a crossover between two dielectric relaxation processes with increasing temperature, which involve polar nanoregions of different phases and which have different temperature evolutions [13]. T_m stands for the temperature corresponding to the maximum value of ε_r. It was previously ascribed to a tetragonal to cubic phase transition [14], while recently it is believed to be linked with a relaxation of tetragonal polar nanoregions (PNRs) emerged from rhombohedral PNRs [15], including two events: (a) the disappearance of the rhombohedral phase (frequency-independent anomaly in permittivity) and (b) the relaxation process of the polar nanoregions with tetragonal symmetry [15]. The frequency dispersive anomaly at T_s can be associated with the relaxation of the polar nanoregion of the rhombohedral phase [15]. Generally, ε_r at T_s is much smaller than that at T_m. However, in this work, we find an interesting phenomenon that the maximum ε_r of BNKT0–100*x*KNN samples deep in pseudocubic phase ($x \geq 0.14$) is not achieved at T_m but T_s. Besides, a stronger frequency dispersion of ε_r is clearly seen for these samples: ε_r at T_s decreases and significantly shifts to higher temperatures as the measurement frequency increases. It seems that the relaxor behavior of the ceramics becomes stronger as the KNN content increases. The dielectric dispersion and diffuseness of the phase transition and the enhanced relaxor behavior can be well illustrated by the modified Curie–Weiss law [16] and the microdomain–macrodomain transition theory [17, 18], which has been reported in our previous work [12].

Moreover, for BNKT20–100*x*KNN ceramics, a plateau of almost constant permittivity is formed for $x = 0.18$ and $x = 0.20$. Taking 170 °C as a reference point, a very high

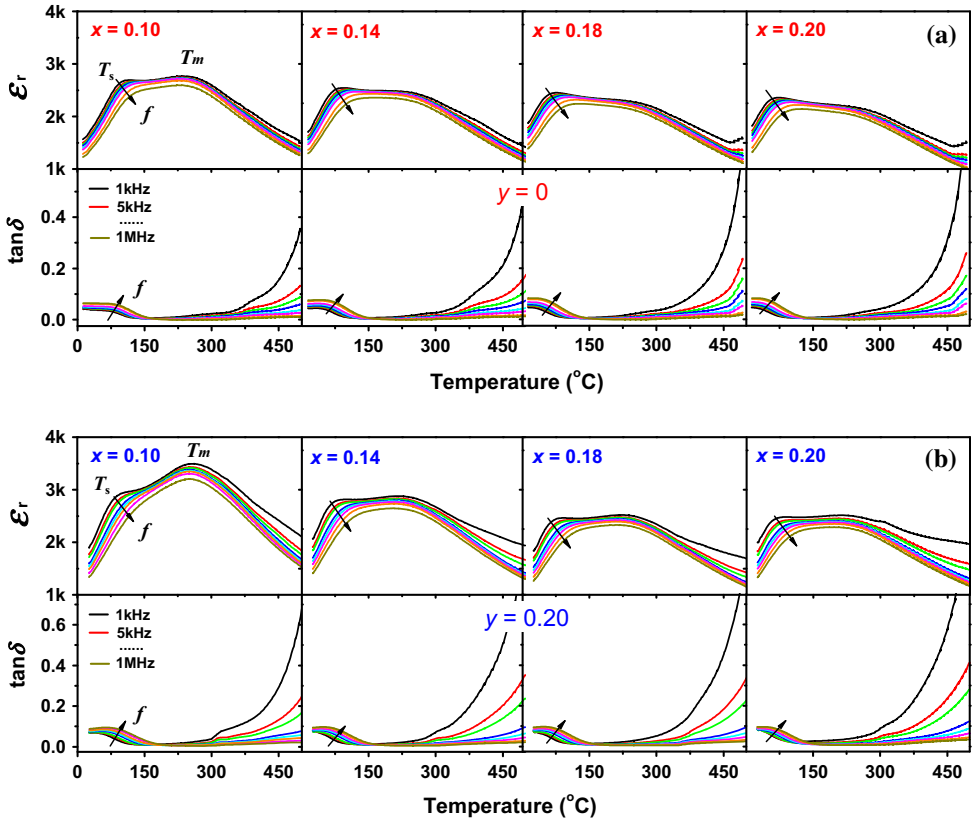

Fig. 4 The frequency dispersion of the dielectric properties of BNKT100*y*–100*x*KNN ($y = 0$, 0.20; $x = 0.10$–0.20) ceramics

permittivity of 2469 (2385) ± 20 % (at 10 kHz) is maintained from room temperature up to at least 420 °C, spanning a range of about 400 °C. This very flat relative permittivity is achieved by a combination of effects [6]. An increasing amount of KNN reduces the relative permittivity at the T_s to a small degree but the relative permittivity at the T_m to a large degree and leads to a smearing out of the T_s. This combination results in nearly temperature-independent relative permittivity characteristic. This is compared to the dependence of strain on temperature in the regime between RT and 180 °C. As predicted through $S = QP^2$, in conjunction with the low dependence of relative permittivity and electrostrictive coefficient with temperature, a very low temperature dependence of strain with less than 8 % from the average value is obtained. In relaxor materials, polarization and relative permittivity are strong functions of temperature leading to large temperature dependence of the strain ($S = QP^2$). However, this is not the case in "AFE" electrostrictors of BNKT100*y*–100*x*KNN investigated here. This will be further studied in Fig. 9.

Figure 5 shows the impedance spectra of the BNKT100*y*–100*x*KNN [(a) $y = 0.20$, $x = 0.10$–0.20; (b) $y = 0$, $x = 0.10$–0.20] ceramics in the frequency range of 0.01 Hz to 20 MHz over 500–650 °C. Commonly, electrode, grain boundary, and grain components contribute to the conductivities of the polycrystalline materials and their effects on conduction can be segregated into three parallel *RC* elements connected in series in an equivalent circuit, from low frequency to high frequency [19, 20]. However, for BNKT20–100*x*KNN ($x = 0.10$–0.20) and BNKT0–100*x*KNN ($x = 0.10$–0.18) samples, only a single, essentially undistorted Debye-like semicircle is observed at each temperature, and these curves can be fitted to the standard semicircles with the grain (R_bC_b) element, as shown in Fig. 5c. This indicates that these compositions contain essentially one electrical component associated with the grain effect. However, for the BNKT0–100*x*KNN ($x = 0.20$) ceramic, distorted Debye-like semicircles at variable temperatures are observed, together with a second electrical component apparent at low frequency range. Also, the distorted semicircle at each temperature can be segregated into two natural electrical components corresponding to the two fitting semicircles in the impedance plots as found in Fig. 5d. The bigger semicircle in the higher frequency range is ascribed to the grain effect, while the grain boundary response contributes to the smaller semicircle in the lower frequency range [20].

Figure 6 plots the lnσ of dc conductivity of BNKT100*y*–100*x*KNN ceramics as a function of reciprocal temperature (1000/*T*) in the temperature range from 550 to 650 °C,

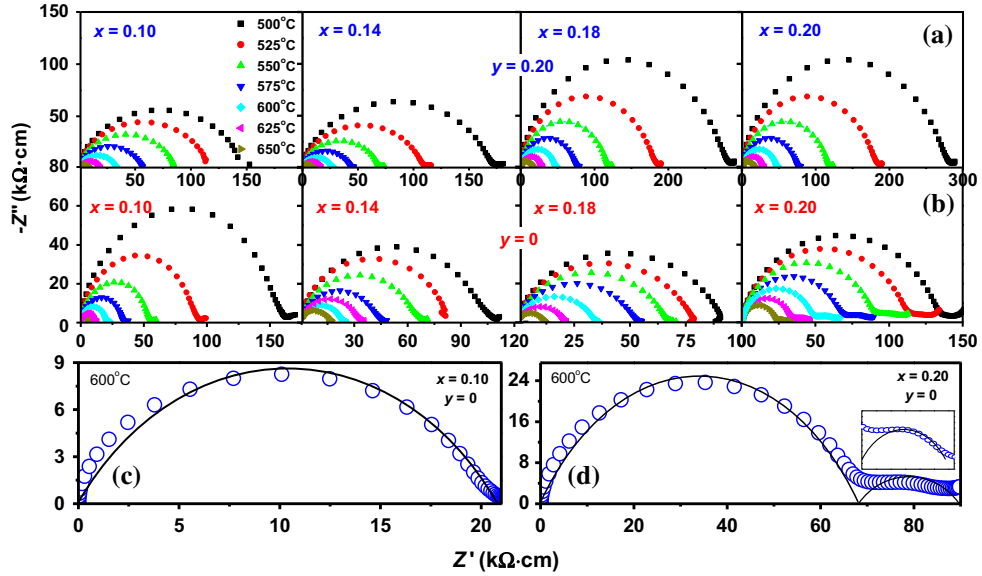

Fig. 5 The impedance spectra of the BNKT100*y*–100*x*KNN **a** $y = 0$, 0.20; **b** $x = 0.10$–0.20 ceramics in the frequency range of 0.01 Hz to 20 MHz over 500–650 °C. **c**, **d** The fitting semicircles in the impedance plots of the KNLN6–*x*BKT ceramics ($y = 0$; $x = 0.10$ and $x = 0.20$)

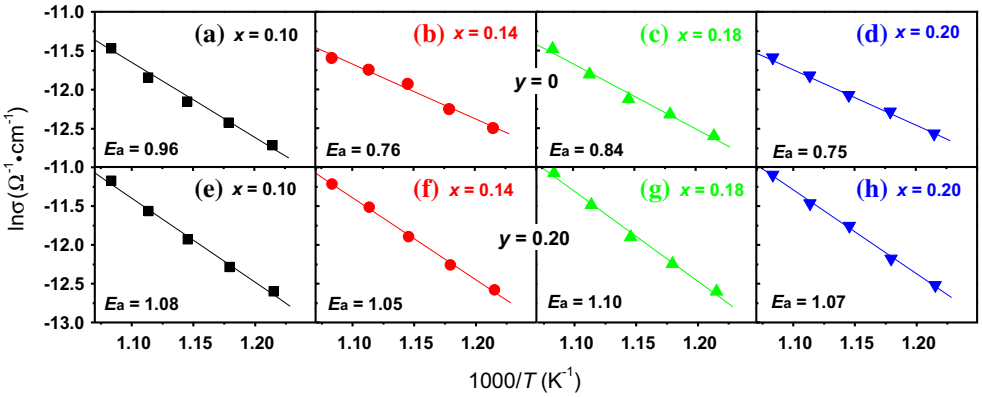

Fig. 6 Plots the lnσ of dc conductivity of BNKT100*y*–100*x*KNN ceramics as a function of reciprocal temperature (1000/*T*)

where the activation energy (E_a) for electrical conduction can be detected by using the following Arrhenius equation [21],

$$\sigma = \sigma_0 \exp(-E_a/kT), \quad (1)$$

where σ and σ_0 are the dc conductivity and the pre-exponent constant, respectively, E_a is the activation energy, k is Boltzmann's constant, and T is absolute temperature. In ABO_3 perovskite materials, the values of E_a for A- and B-site cations are around 4 and 12 eV, respectively [22, 23]. For oxygen vacancies, it varies from 0.5 to 2 eV, depending on their concentration [24]. From Fig. 6, the achieved activation energy (E_a) of BNKT100*y*–100*x*KNN system are in the range of 0.79–1.09 eV, which are closely related to the oxygen ion/vacancy migration [24]. Therefore, it is reasonable to suggest that oxygen vacancies dominate the conductivity in this temperature range from 550 to 650 °C.

Figures 7 illustrates the *P*–*E* loops and *S*–*E* curves of BNKT100*y*–100*x*KNN ($y = 0$, 0.20; $x = 0.10$–0.20) under an electric field of 80 kV/cm at 10 Hz. A "pinched" hysteresis loop with large strain of 0.20 % is observed for BNKT0–10KNN samples. For solid-state actuator application, the electric-field-induced strain is generally required to be accompanied with low hysteresis so as to improve the sensitivity. Although large strain response is obtained in BNKT0–10KNN samples, high hysteresis is accompanied due to the switching process in field-induced ferroelectric order from ergodic relaxor phase [25]. Similar behaviors are commonly found in BNT-based "AFE-like" ceramics [11, 26, 27]. In the present study, we found that the hysteresis behavior is significantly decreased by

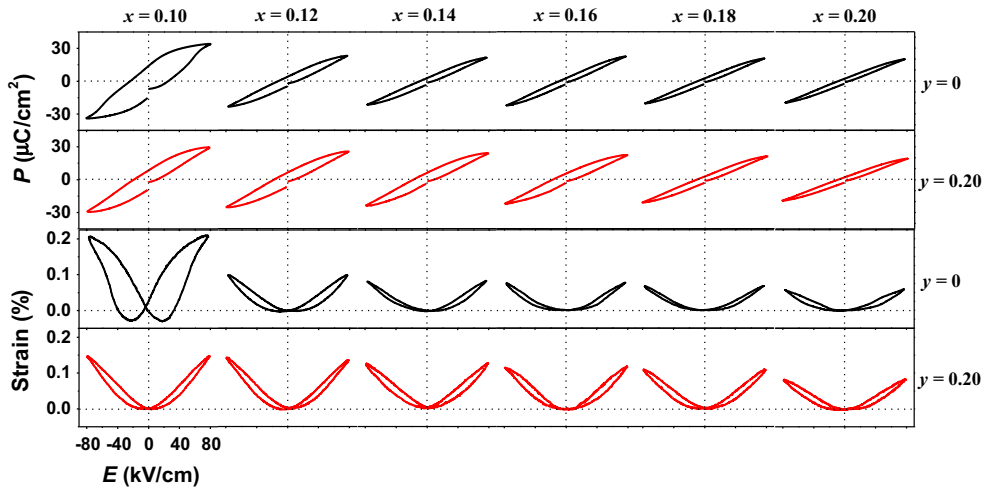

Fig. 7 The *P*–*E* loops and *S*–*E* curves of BNKT100*y*–100*x*KNN ($y = 0$, 0.20; $x = 0.10$–0.20) under an electric field of 80 kV/cm at 10 Hz

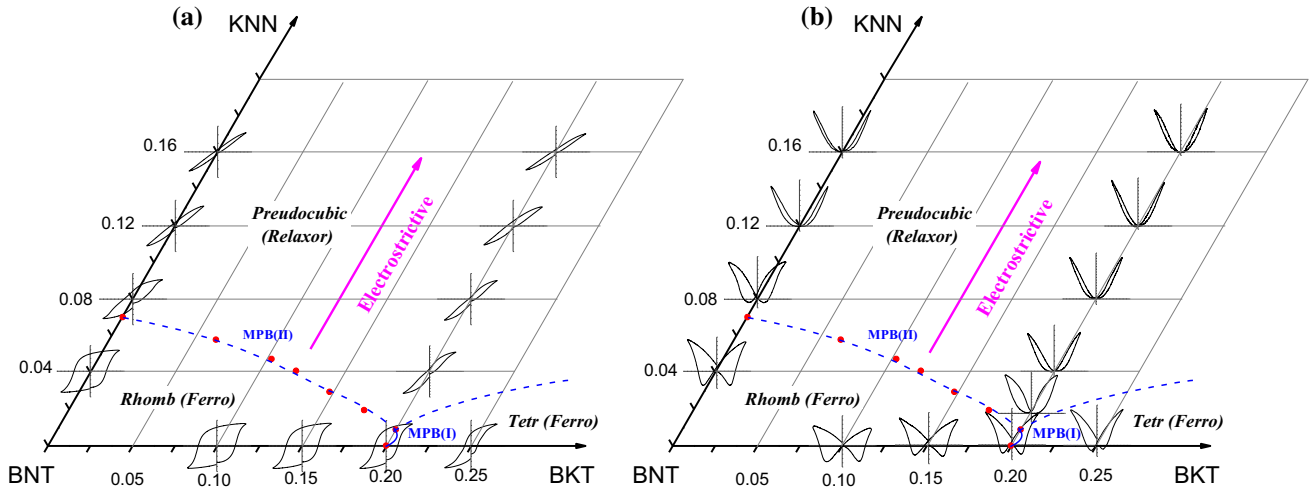

Fig. 8 Change in the **a** *P*–*E* loops and **b** *S*–*E* curves under an electric field of 80 kV/cm at 10 Hz with the composition in ternary BNT–BKT–KNN system

increasing the KNN concentration. Samples of BNKT100*y*–100*x*KNN with high KNN concentration ($x > 0.16$) exhibit very slim *P*–*E* and *S*–*E* profiles and also maintain relative large strain level of 0.10–0.14 %. This strain level is comparable with other lead-containing electrostrictors [6, 8, 28]. So these materials have great potential in the fabrication of high-performance lead-free electrostrictors. The very slim *P*–*E* loops and *S*–*E* curves with small hysteresis are related to the pseudocubic phase of the materials, as clearly illustrated in Fig. 8.

Figure 9a shows the plots of *S* and P^2 derived from the *P*–*E* loops and *S*–*E* curves of Fig. 6, for BNKT100*y*–100*x*KNN system. The slope of this curve corresponds to the electrostriction coefficient Q_{33} [8]. Clearly, the *S*–P^2 curves for the BNKT100*y*–100*x*KNN system with low KNN content ($x = 0.10$–0.14) are slightly deviated from liner relations, which suggests the contribution of electrostriction strain should be predominant while not pure. There apparently still are contributions from ferroelectric switching present and also including the contributions by other types of electromechanical coupling, such as local volume changes due to field-induced relaxor-ferroelectric switching and the piezoelectric effect of the ferroelectric phase [6]. While for BNKT20–100*x*KNN samples with high KNN concentration ($x = 0.16$–0.20) nearly purely electrostrictive behavior occurred owing to rare contributions of electrostriction strain from ferroelectric switching. This result is consistent with the slimmer *P*–*E* profiles which induced the profile of *S* versus P^2 that can be fitted well to a straight line. Figure 9b gives the comparisons of *S*–P^2 curves between the BNKT0–100*x*KNN and BNKT20–100*x*KNN ($x = 0.14$, $x = 0.18$) samples with the same KNN content (x). It can be found that

BNKT20–100xKNN samples have larger stain values than that of BNKT0–100xKNN samples with the same KNN content (x), suggesting that the BKT substitution (y) into BNKT0–100xKNN can effectively enhance the electrostrictive properties of the ceramics. The results can be seen more clearly in Fig. 9c, the variation of electrostrictive coefficient Q_{33} of BNKT100y–100xKNN system as a function x. For BNKT100y–100xKNN samples with $y = 0.20$ and $x = 0.16$, the Q_{33} is calculated to be of 0.025 m^4/C^2, and this value is comparable to the reported PMN-based electrostrictive materials [29] and the promising BNT-based lead-free electrostrictors [30, 31]. In the present work, although two series of compositions were both designed based on the MPB compositions of ternary BNT–BKT–KNN system, as depicted in Fig. 8. The achieved Q_{33} of the two series of compositions are quite different. BNKT20–100xKNN system fabricated based on the MPB(II) composition (BNKT20–1KNN) exhibits much higher Q_{33} values compared with that of BNKT0–100xKNN samples based on the MPB(II) composition (BNKT0–7KNN). We believed that the drastically enhanced Q_{33} of the BNKT20–100xKNN should be ascribed to the large strain response of its initial composition (BNKT20–1KNN), which possesses a giant value of 0.45 % [27]. By contrast, the strain of the initial composition (BNKT0–7KNN) for fabricating BNKT0–100xKNN system is only 0.22 %, and it decreases down to 0.06 % as the KNN content reaches $x = 0.20$. As a result, this system displays a much lower Q_{33}.

This class of materials is not only attractive for room temperature electrostrictive properties, but is predicted to have low temperature dependence in electrostrictive strain

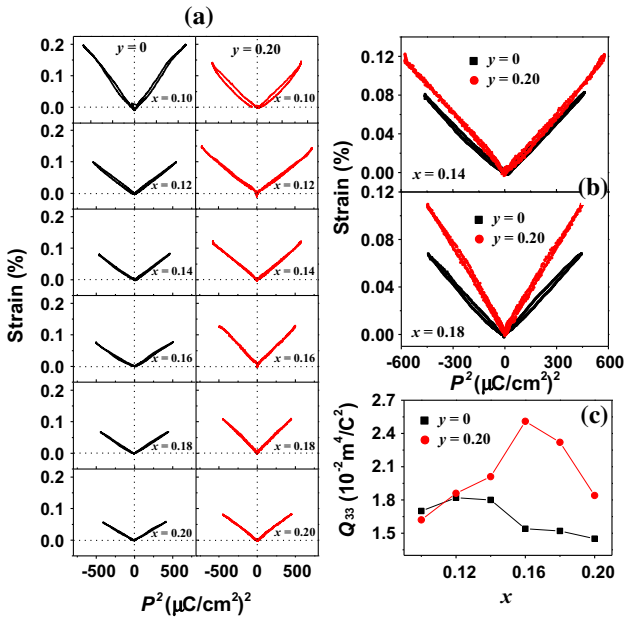

Fig. 9 **a** The plots of S and P^2 derived from the P–E loops and S–E curves under an electric field of 80 kV/cm at 10 Hz, for BNKT100y–100xKNN system, **b** the comparisons of S–P^2 curves between the BNKT0–100xKNN and BNKT20–100xKNN samples with the same KNN content (x), **c** the variation of electrostrictive coefficient Q_{33} as a function x, for BNKT100y–100xKNN samples

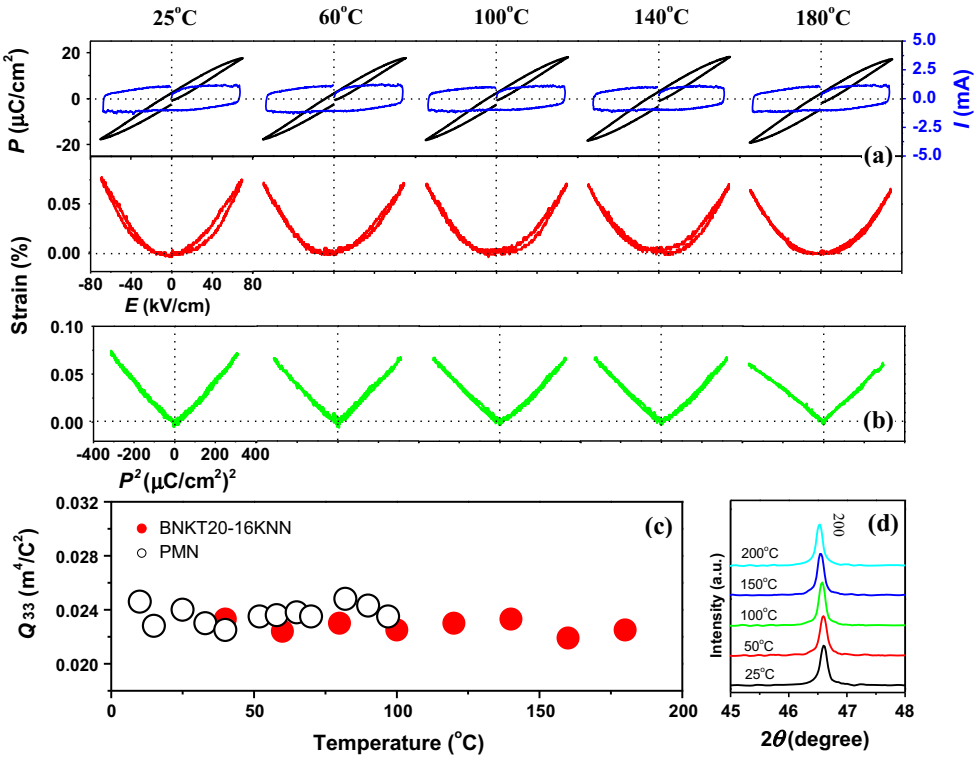

Fig. 10 **a** P–E/I–E loops, S–E, and **b** S–P^2 curves of BNKT20–16KNN at different temperatures under an electric field of 70 kV/cm at 10 Hz, **c** variations of electrostrictive coefficient Q_{33} with temperature for the studied BNKT20–16KNN and the traditional PMN ceramics [2]. **d** The (200) diffraction reflection for the ceramics at selected temperatures

also. Figure 10 exemplarily displays the (a) *P–E/I–E* loops, *S–E*, and (b) S–P^2 curves of BNKT20–16KNN at different temperatures. There was no domain switching current peak in BNKT20–16KNN sample, suggesting no domain switching takes place as confirmed by nearly zero piezoelectric constant d_{33} after poling [32]. The maximum polarization P_m observed in *P–E* loops and the strain reflected *S–E* curves are nearly constant in the temperature range between RT and 180 °C for the case of 10 Hz driving frequency. Consequently, the electrostrictive properties of BNKT20–16KNN samples show little temperature dependence, and the almost flat, temperature-independent characteristic of the BNKT20–16KNN samples is even comparable with traditional PMN [2], since the Q_{33} deterioration value for this sample is only ~7 % between RT and 180 °C (Fig. 10c). Furthermore, temperature-dependent structural analysis of this sample as given in Fig. 10d reveals that the excellent temperature stability of electrostrictive properties should be induced by the stable relaxor pseudocubic phase over a wide temperature range. The XRD patterns with measured temperature provide no phase transitions in the temperatures range of 25–200 °C. Besides minor fluctuations in intensity and a shift in the reflex due to thermal expansion, there is no obvious change of (200) diffraction peak. That is, sample maintains a relaxor pseudocubic phase in the temperature range of 25–200 °C. The electrostrictive behavior of the BNKT20–16KNN is of great importance for temperature-independent actuator devices.

Suitable materials for actuator applications should not only show excellent electrostrictive properties and good temperature stability but also reliability under long-term electric cycling. For BNT-based materials, however, the fatigue behavior did not get much attention so far, even though it is a crucial aspect for industrial implementation. Figure 11a shows the fatigue behavior of BNKT20–20KNN ceramics for 10^5 cycles, and the Q_{33} levels at different fatigue cycles are also summarized in this figure. It can be observed that the BNKT20–16KNN material exhibits no fatigue behavior. Even after switching cycles over 10^5, samples still maintain purely electrostrictive effect with a high electrostrictive coefficient (Q_{33}) of 0.024 m^4/C^2. It can thus be concluded that electrostrictive properties in the BNKT20–16KNN system are extremely stable during the application of the external electric field. To understand the behavior of the electrostrictive strain during electrical cycling more in detail, bipolar hysteresis loops of permittivity ε_r, loss tanδ, polarization P, piezoelectric coefficient d_{33}^*, and strain S (bipolar and unipolar strain) were recorded in the unfatigued state and after distinct cycling steps. Figure 11b–g gives the evolution of ε_r–E, tanδ–E, P–E, d_{33}^*–E, and S–E hysteresis loops of BNKT20–16KNN ceramics. Similarly, all the above electrical parameters were found to be

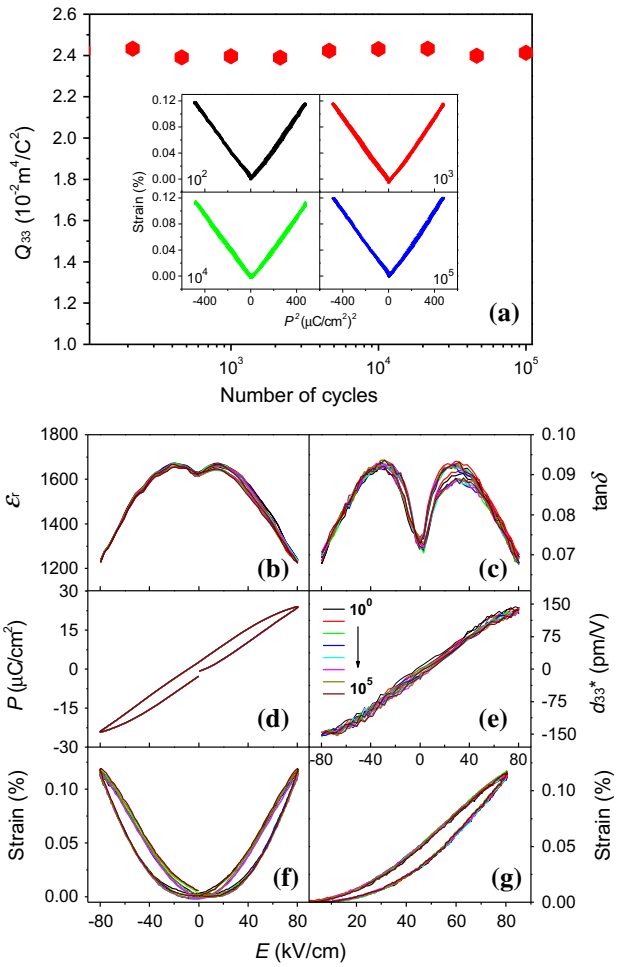

Fig. 11 **a** The fatigue behavior of BNKT20–16KNN ceramics at 10 Hz for 10^5 cycles, insets show the Q_{33} levels and S–P^2 curves at different fatigue cycles. **b–g** The evolution of ε_r–E, tanδ–E, P–E, d_{33}^*–E, and S–E hysteresis loops at 10 Hz of BNKT20–16KNN ceramics with fatigue cycles

independent of the number of electric-field cycles for at least up to 10^5 cycles. The exceptionally good fatigue resistance up to 10^5 unipolar cycles renders this material promising for actuator applications.

Conclusions

In summary, based on the MPB composition of BNT–BKT–KNN ceramics, we designed a series of compositions which lie deep in the pseudocubic region of ternary BNT–BKT–KNN system. By changing the content of BKT and KNN, a high, purely electrostrictive effect was developed in BNKT20–20KNN samples, which shows an electrostrictive coefficient Q_{33} of 0.025 m^4/C^2 comparable with that of traditional Pb-based electrostrictors. Furthermore, this material can deliver an exceptionally good fatigue

resistance and provide temperature independence of strain, indicating great potential in environmental-friendly solid-state actuators.

Acknowledgements This work was supported by the National Natural Science Foundation of China (Nos. 51402144, 51372110, 51302124), the Project of Shandong Province Higher Educational Science and Technology Program (Grant Nos. J14LA11 and J14LA10), the National High Technology Research and Development Program of China (No. 2013AA030801), Science and Technology Planning Project of Guangdong Province, China (No. 2013B091000001), Independent innovation and achievement transformation in Shandong Province special, China (No. 2014CGZH0904), the Natural Science Foundation of Shandong Province of China (No. ZR2012EMM004), and the Research Foundation of Liaocheng University (Nos. 318051407, 318011301, 318011306).

References

1. Haertling GH (1999) Ferroelectric ceramics: history and technology. J Am Ceram Soc 82:797–818
2. Kuwata J, Uchino K, Nomura S (1980) Electrostrictive coefficients of $Pb(Mb_{1/3}Nb_{2/3})O_3$ Ceramics. Jpn J Appl Phys 19:2099–2103
3. Ealey MA, Moore DM, Anderson EH, Fanson JL (1990) Development of an active truss element for control of precision structures. Opt Eng 29:1333–1341
4. Jaffe B, Cook W, Jaffe H (1971) Piezoelectric ceramics. Academic Press, New York
5. Zhang ST, Yan F, Yang B, Cao WW (2010) Phase diagram and electrostrictive properties of $Bi_{0.5}Na_{0.5}TiO_3$-$BaTiO_3$-$K_{0.5}Na_{0.5}NbO_3$ ceramics. Appl Phys Lett 97:122901
6. Zhang ST, Kounga AB, Jo W, Jamin C, Seifert K, Granzow T, Rödel J, Damjanovic D (2009) High-strain lead-free antiferroelectric electrostrictors. Adv Mater 21:4716–4720
7. Bobnar V, Malič B, Holc J, Kosec M, Steinhausen R, Beige H (2005) Electrostrictive effect in lead-free relaxor $K_{0.5}Na_{0.5}NbO_3$-$SrTiO_3$ ceramics system. J Appl Phys 98:024113
8. Ang C, Yu Z (2006) High, purely electrostrictive strain in lead-free dielectrics. Adv Mater 18:103–106
9. Hao JG, Wang JW, Bai WF, Shen B, Zhai JW (2012) Switching of morphotropic phase boundary and large electrostrictive effect in lead-free BNT–BKT–KNN ceramics. Phys Status Solidi RRL 6:451–453
10. Tran VDN, Han HS, Yoon CH, Lee JS, Jo W, Rödel J (2011) Thermally stable field-induced strain of lead-free electrostrictive Bi-based perovskite ceramics. Mater Lett 65:2607–2609
11. Hao JG, Shen B, Zhai JW, Liu CZ, Li XL, Gao ZY (2013) Switching of morphotropic phase boundary and large strain response in lead-free ternary $(Bi_{0.5}Na_{0.5})TiO_3$–$(K_{0.5}Bi_{0.5})TiO_3$–$(K_{0.5}Na_{0.5})NbO_3$ system. J Appl Phys 113:114106
12. Hao JG, Bai WF, Li W, Shen B, Zhai JW (2012) Phase transitions, relaxor behavior, and electrical properties in $(1-x)(Bi_{0.5}Na_{0.5})TiO_3$–$x(K_{0.5}Na_{0.5})NbO_3$ lead-free piezoceramics. J Mater Res 27:2943–2955
13. Viola G, McKinnon R, Koval V, Adomkevicius A, Dunn S, Yan HX (2014) Lithium-induced phase transitions in lead-free $Bi_{0.5}Na_{0.5}TiO_3$ based ceramics. J Phys Chem C 118:8564–8570
14. Hiruma Y, Nagata H, Takenaka T (2009) Detection of morphotropic phase boundary of solid-solution ceramics. Appl Phys Lett 95:052903
15. Jo W, Schaab S, Sapper E, Schmitt LA, Kleebe HJ, Bell AJ, Rödel J (2011) On the phase identity and its thermal evolution of lead free $(Bi_{1/2}Na_{1/2})TiO_3$-6 mol% $BaTiO_3$. J Appl Phys 110:074106
16. Uchino K, Nomura S (1982) Critical exponents of the dielectric constants in diffused phase transition crystals. Ferroelectr Lett Sect 44:55–61
17. Zhang DJ, Yao X (2004) Dynamics on microdomain-macrodomain transition of relaxor ferroelectrics. Acta Phys Chim Sin 20:712–716
18. Gao F, Liu LL, Xu B, Hu GX, Cao X, Hong RZ, Tian CS (2011) Platelike $NaNbO_3$ particles were used as templates to fabricate grain-oriented $0.96(0.8Na_{0.5}Bi_{0.5}TiO_3$–$0.2K_{0.5}Bi_{0.5}TiO_3)$ –$0.04NaNbO_3$ (NKBT) ceramics. J Eur Ceram Soc 31:2987–2996
19. Irvine JTS, Sinclair DC, West AR (1990) Electroceramics: characterisation by impedance spectroscopy. Adv Mater 2:132–138
20. Sinclair DC, West AR (1989) Impedance and modulus spectroscopy of semiconducting $BaTiO_3$ showing positive temperature coefficient of resistance. J Appl Phys 66:3850
21. Deng GC, Li GR, Ding AL, Yin QR (2005) Evidence for oxygen vacancy inducing spontaneous normal-relaxor transition in complex perovskite ferroelectrics. Appl Phys Lett 87:192905
22. Kang BS, Chol SK, Park CH (2003) Diffuse dielectric anomaly in perovskite-type ferroelectric oxides in the temperature range of 400–700 °C. J Appl Phys 94:1904
23. Raymond MV, Smyth DM (1996) Defects and charge transport in perovskite ferroelectrics. J Phys Chem Solids 57:1507–1511
24. Steinsvik S, Bugge R, Gjonnes J, Tafto J, Norby T (1997) The defect structure of $SrTi_{1-x}Fe_xO_{3-y}$ ($x = 0$–0.8) investigated by electrical conductivity measurements and electron energy loss spectroscopy (EELS). J Phys Chem Solids 58:969–979
25. Jo W, Dittmer R, Acosta M, Zang JD, Groh C, Sapper E, Wang K, Rödel J (2012) Giant electric-field-induced strains in lead-free ceramics for actuator applications—status and perspective. J Electroceram 29:71–93
26. Wang FF, Xu M, Tang YX, Wang T, Shi WZ, Leung CM (2012) Large strain response in the ternary $Bi_{0.5}Na_{0.5}TiO_3$–$BaTiO_3$–$SrTiO_3$ solid solutions. J Am Ceram Soc 95:1955–1959
27. Hao JG, Bai WF, Li W, Shen B, Zhai JW (2013) Phase transitions, relaxor behavior and large strain response in $LiNbO_3$-modified $Bi_{0.5}(Na_{0.80}K_{0.20})_{0.5}TiO_3$ lead-free piezoceramics. J Appl Phys 114:044103
28. Jiang WH, Cao WW (2000) Intrinsic and coupling-induced elastic nonlinearity of lanthanum-doped lead magnesium niobate–lead titanate electrostrictive ceramic. Appl Phys Lett 77:1387
29. Furuta A, Uchino K (1993) Dynamic observation of crack propagation in piezoelectric multilayer actuators. J Am Ceram Soc 76:1615–1617
30. Bai WF, Li LY, Wang W, Shen B, Zhai JW (2015) Phase diagram and electrostrictive effect in BNT-based ceramics. Solid State Commun 206:22–25
31. Bai WF, Li LY, Li W, Shen B, Zhai JW, Chen H (2014) Phase diagrams and electromechanical strains in lead-free BNT-based ternary perovskite compounds. J Am Ceram Soc 97:3510–3518
32. Yan HX, Inam F, Viola G, Ning H, Zhang HT, Jiang QH, Zeng T, Gao ZP, Reece MJ (2011) The contribution of electrical conductivity, dielectric permittivity and domain switching in ferroelectric hysteresis loops. J Adv Dielectr 1:107–118